Supporting Information for

Bioinspired Di-Fe Complexes: Correlating Structure and Proton Transfer over Four Oxidation States

Justin L. Lee, Saborni Biswas, Chen Sun, Joseph W. Ziller, Michael P. Hendrich,* A. S. Borovik*

Table of Content

General Methods. All reagents were purchased from commercial sources and used as received unless otherwise noted. Solvents were sparged with argon and purified using a JC Meyer Co. solvent purification system with columns containing Q-5 and molecular sieves. Butyronitrile (PrCN) was purified according to a literature procedure.[1] Potassium hydride (KH) as a 30 % dispersion in mineral oil was filtered with a medium porosity glass frit and washed 5 times each with pentane and diethyl ether (Et_2O). Solid KH was dried under vacuum and stored under an inert atmosphere. All synthetic manipulations were conducted in a Vacuum Atmosphere, Co. drybox under an argon atmosphere. $K[Fe^{III}poat(OH)]$,[2] $K[Fe^{II}poat]$,[3] $[Fe^{II}(TMTACN)(OTf)_2]$,[4] $[FeCp_2]OTf$,[5] IBX-iPr,[6,7] 2,6-lutidinium triflate,[8] and $[N(p\text{-}C_6H_4Br)_3]PF_6$[9,10] were synthesized according to previous reports. Triethylamine (NEt_3) was purified by vacuum distillation. 2,6-di-*tert*-butyl-phenol (DTBP) was purified by recrystallization in absolute ethanol twice. The ^{57}Fe-enriched complexes were prepared

using $^{57}Fe^{II}(OAc)_2$ and $^{57}Fe^{II}(OTf)_2 \cdot 2CH_3CN$, which were synthesized according to procedures for the natural abundance Fe precursors.[11,12]

Physical Methods. Room temperature electronic absorbance spectra were recorded with a Cary 50 using a 1.00 cm quartz cuvette. Low temperature electronic absorbance spectra were recorded on an Agilent UV-vis spectrophotometer equipped with a Unisoku Unispeks cryostat in a 1.00 cm quarts cuvette. High resolution mass spectra were collected using Waters Micromass LCT Premier Mass Spectrometer. Solid-state Fourier transform infrared (FTIR) spectra were collected on a Thermo Scientific Nicolet iS5 FT-IR spectrometer equipped with an iD5 ATR accessory. Cyclic voltammetric experiments were conducted using a CHI600G electrochemical analyzer. A 2.0 mm glassy carbon electrode was used as the working electrode at scan velocities between 2 and 2000 mV s^{-1}. A ferrocenium/ferrocene ($[FeCp_2]^{+/0}$) or an acetylferrocenium/acetylferrocene ($[AcFc]^{+/0}$, + 0.27 V versus $[FeCp_2]^{+/0}$)[5] was used as an internal reference to monitor the reference electrode (Ag^+/Ag). Tetrabutylammonium hexafluorophosphate (TBAP) was used as the supporting electrolyte at a concentration of 0.1 M in CH_2Cl_2 or PrCN. Elemental analyses were performed on a Perkin-Elmer 2400 Series II CHNS elemental analyzer. ^1H–NMR spectra was collected on a Bruker CRYO500 spectrometer (500 MHz). Organic products were detected by gas-chromatography mass spectrometry (GC-MS) in the Mass Spectrometry Facility at the University of California, Irvine. The GC-MS was a Trace 1300 Gas Chromatograph from Thermo Scientific using a 15 m long x 0.25 mm i.d. TG-SQC column. The oven was held at 40 °C for 1 minute then heated at a rate of 20 °C min^{-1} to 290 °C and held for an additional 2 minutes. The mass spectrometry used electron ionization (70 eV) scanning (0.2/sec) from m/z 30 – 650.

EPR spectra were recorded on a Bruker ELEXSYS spectrometer equipped with an Oxford ESR-910 liquid helium cryostat and a Bruker bimodal cavity for the generation of microwave fields parallel and transverse to the applied magnetic field. The quantification of all signals was performed relative to a CuEDTA spin standard prepared from a copper atomic absorption standard (Sigma-Aldrich). The microwave frequency was calibrated with a frequency counter, and the magnetic field

was measured with an NMR gaussmeter. The sample temperature was calibrated against a calibrated cernox sensor (Lakeshore CX-1050) mounted inside an EPR tube. A modulation frequency of 100 kHz was used for all EPR spectra. Mössbauer spectra were recorded on a weak-field spectrometer operating in a constant acceleration mode in a transmission geometry using Janis Research Inc. cryostat that allows for a variation in temperature from 4 to 300 K. Isomer shifts are reported relative to Fe metal at 298 K. Assignments are made by the coordination geometry differences and in comparison with properties of the mononuclear Fe(II) and Fe(III) analogues. We will report these findings in an upcoming manuscript.

Crystallography.

[(TMTACN)Fe^{II}–(μ-OH)–Fe^{III}poat]OTf. A yellow crystal of approximate dimensions 0.142 x 0.213 x 0.306 mm was mounted in a cryoloop and transferred to a Bruker SMART APEX II diffractometer system. The APEX2[13] program package was used to determine the unit-cell parameters and for data collection (45 sec/frame scan time). The raw frame data was processed using SAINT[14] and SADABS[15] to yield the reflection data file. Subsequent calculations were carried out using the SHELXTL[16] program package. There were no systematic absences nor any diffraction symmetry other than the Friedel condition. The centrosymmetric triclinic space group $P\bar{1}$ was assigned and later determined to be correct.

The structure was solved by direct methods and refined on F^2 by full-matrix least-squares techniques. The analytical scattering factors[17] for neutral atoms were used throughout the analysis. There were two molecules of the formula-unit present (Z = 4). Hydrogen atoms H(1) and H(5) were located from a difference-Fourier map and refined (x,y,z and U_{iso}). The remaining hydrogen atoms were included using a riding model. Several atoms were disordered and included using multiple components with partial site-occupancy-factors. Least-squares analysis yielded wR2 = 0.1027 and

Goof = 1.020 for 1581 variables refined against 31868 data (0.69 Å), R1 = 0.0434 for those 22037 data with $I > 2.0\sigma(I)$.

[(TMTACN)Fe^{III}–(μ-O)–Fe^{III}Hpoat](OTf)$_2$. A brown crystal of approximate dimensions 0.216 x 0.242 x 0.313 mm was mounted on a glass fiber and transferred to a Bruker SMART APEX II diffractometer system. The APEX2[13] program package was used to determine the unit-cell parameters and for data collection (20 sec/frame scan time). The raw frame data was processed using SAINT[14] and SADABS[15] to yield the reflection data file. Subsequent calculations were carried out using the SHELXTL[16] program package. The diffraction symmetry was 2/*m* and the systematic absences were consistent with the monoclinic space group $P2_1/c$ that was later determined to be correct.

The structure was solved by dual space methods and refined on F^2 by full-matrix least-squares techniques. The analytical scattering factors[17] for neutral atoms were used throughout the analysis. Hydrogen atom H(2) was located from a difference-Fourier map and refined (x,y,z and U_{iso}). The remaining hydrogen atoms were included using a riding model. Several atoms were disordered and included using multiple components with partial site-occupancy-factors. There was one molecule of chloroform solvent present.

Least-squares analysis yielded wR2 = 0.0979 and Goof = 1.022 for 872 variables refined against 18665 data (0.72 Å), R1 = 0.0401 for those 14338 data with $I > 2.0\sigma(I)$. There were several high residuals present in the final difference-Fourier map. It was not possible to determine the nature of the residuals although it was probable that *n*-hexane solvent was present. The SQUEEZE[18a] routine in the PLATON[19b] program package was used to account for the electrons in the solvent accessible voids.

[(TMTACN)Fe^{III}–(μ-O)–Fe^{III}poat]OTf. A red crystal of approximate dimensions 0.236 x 0.265 x 0.266 mm was mounted in a cryoloop and transferred to a Bruker SMART APEX II diffractometer

system. The APEX2[13] program package was used to determine the unit-cell parameters and for data collection (60 sec/frame scan time). The raw frame data was processed using SAINT[14] and SADABS[15] to yield the reflection data file. Subsequent calculations were carried out using the SHELXTL[16] program package. There were no systematic absences nor any diffraction symmetry other than the Friedel condition. The centrosymmetric triclinic space group $P\bar{1}$ was assigned and later determined to be correct.

The structure was solved by direct methods and refined on F^2 by full-matrix least-squares techniques. The analytical scattering factors[17] for neutral atoms were used throughout the analysis. Hydrogen atoms were included using a riding model. There were two molecules of dichloromethane solvent present. One of the chlorine atoms was disordered and included using two components with partial site-occupancy-factors. Least-squares analysis yielded wR2 = 0.1473 and Goof = 1.073 for 737 variables refined against 17414 data (0.70 Å), R1 = 0.0539 for those 13231 data with I > 2.0σ(I).

Preparation of [(TMTACN)Fe^{II}–(*μ*-OH)–Fe^{III}poat]OTf. K[Fe^{III}poat(OH)] (114.9 mg, 0.1343 mmol) was dissolved in 4 mL anhydrous CH_2Cl_2. NMe_4OAc (19.8 mg, 0.149 mmol) was added in one portion, and the mixture was allowed to stir for one hour. The reaction mixture was filtered with a fine porosity glass frit, and the filtrate was added dropwise to a 1 mL CH_2Cl_2 solution of [Fe^{II}(TMTACN)$(OTf)_2$] (70.7 mg, 0.135 mmol). The reaction was allowed to proceed for one hour, and the mixture was filtered with a medium porosity glass frit to remove any insoluble materials. The filtrate was layered with Et_2O to yield a light brown powder. After the light brown powder was collected and dried, it was redissolved in CH_2Cl_2, and was layered with pentane to yield yellow sheet-like crystals. The crystals were collected on a glass frit and dried under vacuum, affording the product in yields that ranged from 45-60 %. Elemental analysis calcd. (found) for [(TMTACN)Fe^{II}–(*μ*-OH)–Fe^{III}poat]OTf·$0.5C_5H_{12}$, $C_{52}H_{64}F_3Fe_2N_7O_7P_3S \cdot 0.5C_5H_{12}$; C, 53.27 (53.33); H, 5.74 (5.52); N, 7.98 (7.98) %. UV-Vis (CH_2Cl_2 solution λ_{max}/nm (ε_{max}/$M^{-1}cm^{-1}$)) 315 (sh), 372 (6400), 460 (sh), 520 (sh). FTIR (ATR, cm^{-1}): 3141(OH), 3062, 3049, 3008, 2991, 2964, 2900, 2866, 2848, 2817, 1591,

1485, 1483, 1464, 1435, 1363, 1265, 1223, 1140, 1115, 1082, 1063, 1030, 1014, 989, 964, 931, 891, 812, 750, 723, 696, 634. $E_{1/2}$ (CH_2Cl_2, V versus $[FeCp_2]^{+/0}$): -1.62 , (i_{pc}/i_{pa} = 1.03, ΔE = 0.23 V, ΔE($[FeCp(\eta\text{-}C_5H_4COMe)]^{+/0}$) = 0.17 V), -0.42 ($i_{pc}/i_{pa}$ = 0.99, ΔE = 0.23 V, ΔE($[FeCp(\eta\text{-}C_5H_4COMe)]^{+/0}$) = 0.17 V).

Preparation of [(TMTACN)Fe^{II}–(μ-OH)–Fe^{II}poat]. [(TMTACN)Fe^{II}–(μ-OH)–Fe^{III}poat]OTf (6.1 mg, 0.0051 mmol) was dissolved in 1.0 mL anhydrous CH_2Cl_2, and solid $CoCp^*_2$ (2.5 mg, 0.0076 mmol) was added in one portion to the brown solution. The solution turned dark orange and was allowed to stir for 1 hour. An aliquot of 250 μL solution was added to an EPR tube via a syringe, and the sample (5.0 mM) was frozen in liquid nitrogen. An aliquot of 60 μL metal solution was diluted by 3.0 mL CH_2Cl_2, and the mixture was transferred into a 1-cm quartz cuvette, which was sealed with a rubber septum and measured by a UV-Vis spectrometer. The synthesis of [$^{57}Fe^{II}$(OH)$^{57}Fe^{II}$poat] was achieved using the same method with the following modifications: 96% ^{57}Fe-enriched [$^{57}Fe^{II}$(OH)$^{57}Fe^{III}$poat]OTf (15.1 mg, 0.0126 mmol) and $CoCp^*_2$ (5.0 mg, 0.015 mmol) were reacted in 2.53 mL PrCN.

Preparation of [(TMTACN)Fe^{III}–(μ-O)–Fe^{III}Hpoat](OTf)$_2$. [(TMTACN)Fe^{II}–(μ-OH)–Fe^{III}poat]OTf (95.0 mg, 0.0796 mmol) was dissolved in 3 mL anhydrous CH_2Cl_2, and solid $[FeCp_2]$OTf (27.8 mg, 0.0830 mmol) was added in one portion to the brown solution. The solution immediately turned dark red, and was allowed to stir for 1.5 hours. All volatiles were then removed under vacuum. The residues were triturated with 20 mL pentane, which was then removed by decanting; the washing process was repeated four times. The residues were redissolved in 6 mL CH_2Cl_2, which was layered with pentane to yield orange needle-like crystals. The crystals were collected on a glass frit and washed with pentane and Et_2O. The crystals were then dried under vacuum, affording the product in yields that ranged from 90-95 %. Elemental analysis calcd. (found) for [(TMTACN)Fe^{III}–(μ-O)–Fe^{III}Hpoat](OTf)$_2$·1.5CH_2Cl_2, $C_{53}H_{64}F_6Fe_2N_7O_{10}P_3S_2$·1.5$CH_2Cl_2$; C,

44.55 (44.54); H, 4.60 (4.38); N, 6.67 (6.92) %. UV-Vis (CH_2Cl_2 solution λ_{max}/nm (ε_{max}/$M^{-1}cm^{-1}$)) 380 (7000), 517 (970), 705 (130). FTIR (ATR, cm^{-1}): 3224 (NH), 3078, 3055, 3012, 2902, 2864, 2823, 1591, 1495, 1473, 1464, 1437, 1360, 1255, 1223, 1140, 1119, 1070, 1055, 1028, 1009, 989, 968, 930, 918, 897, 854, 814, 748, 725, 696, 634. ESI-MS (CH_3CN, ES^+, m/z): exact mass calcd for $[Fe^{III}(O)Fe^{III}Hpoat(OTf)]^+$, $C_{52}H_{64}F_3Fe_2N_7O_7P_3S$, 1192.2455; found, 1192.2485.

Preparation of [(TMTACN)Fe^{III}–(μ-O)–Fe^{III}poat]OTf. K[Fe^{II}poat] (121.4 mg, 0.1447 mmol) and 18-crown-6 (76.8 mg, 0.291 mmol) were dissolved in 7 mL anhydrous THF and 1 mL anhydrous DMF. The yellow solution was transferred to a 50 mL Schlenk flask, which was sealed with a septum and cooled in a -75 °C cold bath outside the glovebox for at least 15 minutes. A 2 mL DMF solution of IBX-iPr (57.8 mg, 0.179 mmol), prepared in the glovebox, was added dropwise into the Schlenk flask via syringe. The reaction mixture immediately turned red, indicative of the formation of $[Fe^{IV}poat(O)]^-$, and was allowed to stir for 20 minutes. A 0.6 mL DMF solution of $[Fe^{II}(TMTACN)(OTf)_2]$ (80.1 mg, 0.152 mmol), prepared in the glovebox, was then added dropwise into the Schlenk flask via syringe. The reaction mixture turned brownish red gradually, and was allowed to stir for 1.5 hours. The Schlenk flask was then warmed up to room temperature, and all volatiles were removed under vacuum. The flask was transferred back in a glovebox, where the residue was redissolved in CH_2Cl_2 and was layered with diethyl ether to yield a brown powder over three days. After the brown powder was collected and dried, it was redissolved in CH_2Cl_2, and was layered with pentane to yield dark red crystalline needles. The crystals were collected on a glass frit and dried under vacuum, affording the product in yields that ranged from 45-55 %. Elemental analysis calcd. (found) for [(TMTACN)Fe^{III}–(μ-O)–Fe^{III}poat]OTf·CH_2Cl_2·C_5H_{12}, $C_{52}H_{63}F_3Fe_2N_7O_7P_3S$·$CH_2Cl_2$·$C_5H_{12}$; C, 51.65 (51.56); H, 5.75 (5.40); N, 7.27 (7.49) %. UV-Vis (CH_2Cl_2 solution λ_{max}/nm (ε_{max}/$M^{-1}cm^{-1}$)) 349 (9200), 531 (780), 780 (250). FTIR (ATR, cm^{-1}): 3070, 3053, 3033, 3008, 2956, 2933, 2898, 2885, 2856, 2844, 1589, 1572, 1500, 1464, 1435, 1390, 1381, 1354, 1276, 1271, 1257, 1227, 1190, 1151, 1147, 1115, 1076, 1066, 1057, 1041, 1032, 1012, 987, 955, 938, 922, 897, 872, 858, 822, 793, 748, 719, 696, 636. ESI-MS (CH_3CN, ES^+, m/z): exact mass calcd

for $[Fe^{III}(O)Fe^{III}poat]^+$, $C_{51}H_{63}Fe_2N_7O_4P_3$, 1042.2856; found, 1042.2855. $E_{1/2}$ (CH_2Cl_2, V versus $[FeCp_2]^{+/0}$): +0.55.

Low-temperature UV-vis solution studies. In a typical experiment, a 10 mM solution of the diiron compound was prepared in CH_2Cl_2 at room temperature and kept in a -35 °C freezer for the duration of the experiment. A 30 - 60 μL aliquot of stock metal complex was added via air-tight syringe to the solvent mixture (3 mL) in a 1-cm quartz cuvette to give the desired concentration for oxidation experiments (0.10 – 0.20 mM). The cuvette was then sealed with a rubber septum and precooled to the desired temperature in an 8453 Agilent UV-vis spectrophotometer equipped with an Unisoku Unispeks cryostat. The solution of metal complex was allowed to equilibrate to the desired temperature for at least 15 min. Stock solutions of other reagents were prepared at concentrations between 10 and 100 mM in the same solvent and added via gas-tight syringe. Reactions were monitored spectrophotometrically by UV-vis spectroscopy.

Low-temperature EPR solution studies. In a typical experiment to generate $[Fe^{III}(OH)Fe^{III}poat]^{2+}$, a 5.8 mM solution (1.97 mL) of $[Fe^{II}(OH)Fe^{III}poat]OTf$ (0.0135 g, 0.0113 mmol) was prepared in the desired solvent at room temperature in a glovebox under argon atmosphere, and kept in a -35 °C freezer for the duration of the experiment. A 200 μL aliquot of stock metal complex (0.00115 mmol, 1.00 equiv) was added via syringe to a quartz EPR tube. The tube was then sealed with a rubber septum and precooled to the desired temperature in -78 °C cold bath outside the glovebox, allowing the solution to equilibrate to the desired temperature for at least 15 min. A 1 mL stock solution of $[FeCp_2]OTf$ was prepared at 46 mM (0.0154 g, 0.0460 mmol) in CH_2Cl_2, and a 30 μL aliquot (0.00138 mmol, 1.25 equiv) added via a gas-tight syringe. The reaction was allowed to incubate for 5 minutes before freezing in liquid nitrogen. The synthesis of $[Fe^{III}(O)Fe^{IV}poat]^{2+}$ was achieved using the same method with the following modifications: 200 μL

of 6.5 mM [Fe^{III}(O)Fe^{III}poat]OTf solution (0.0013 mmol, 1.0 equiv) and an additional 30 μL CH_2Cl_2 were reacted with 30 μL of 43.3 mM [N(*p*-$C_6H_4Br)_3$]PF_6 solution (0.0013 mmol, 1.0 equiv) at -94 °C.

Room-temperature Mössbauer studies. The Mössbauer samples for [$^{57}Fe^{II}$(OH)$^{57}Fe^{III}$poat]$^+$, [$^{57}Fe^{III}$(O)$^{57}Fe^{III}$Hpoat]$^{2+}$, and [$^{57}Fe^{III}$(O)$^{57}Fe^{III}$poat]$^+$ were prepared at room temperature. In a typical experiment, a 5 mM solution of the 96% ^{57}Fe-enriched diiron compound was prepared, and was transferred into a Mössbauer cup before freezing in liquid nitrogen. For the solid sample of [$^{57}Fe^{III}$(O)$^{57}Fe^{III}$Hpoat](OTf)$_2$, ~ 20 mg of the complex was added to the bottom of a Mössbauer cup in an even layer. Anhydrous Nujol mull was added until it reached the top of the sample holder, which was then frozen in liquid nitrogen. The preparation for [$^{57}Fe^{II}$(OH)$^{57}Fe^{II}$poat] is discussed above.

Low-temperature Mössbauer solution studies. In a typical experiment to generate [$^{57}Fe^{III}$(OH)$^{57}Fe^{III}$poat]$^{2+}$, a 5.5-mM solution of the 96% ^{57}Fe-enriched [$^{57}Fe^{II}$(OH)$^{57}Fe^{III}$poat]OTf (0.0074 g, 0.0062 mmol, 1.12 mL) was prepared in PrCN at room temperature in a glovebox under argon atmosphere, and kept in a -35 °C freezer for the duration of the experiment. A 1.0 mL aliquot of stock metal complex (0.0055 mmol) was added via syringe to a 1-cm quartz. The cuvette was then sealed with a rubber septum and precooled to -80 °C in a Unisoku Unispeks cryostat typically used for UV-vis experiments outside the glovebox. The solution of metal complex was allowed to equilibrate to the desired temperature for at least 20 min. A stock solution of [$FeCp_2$]OTf was prepared at 66 mM in PrCN, and an aliquot of the oxidant (0.0066 mmol, 0.10 mL) was added via a gas-tight syringe. Upon completion of the reaction, the septum was sliced open with a razor under a strong flow of argon. The rubber septum was removed and the content in the cuvette was quickly poured into liquid nitrogen. The frozen solid was ground into fine powder and then packed into pre-cooled Mössbauer cups. The synthesis of [$^{57}Fe^{III}$(O)$^{57}Fe^{IV}$poat]$^{2+}$ was achieved using the same

method with the following modifications: 1.5 mL of 5.5 mM [$^{57}Fe^{III}(O)^{57}Fe^{III}$poat]OTf solution (9.9 mg, 0.0083 mmol) was reacted with 0.15 mL of 83 mM [$N(C_6H_4Br)_3$]PF_6 solution (7.8 mg, 0.012 mmol) at -94 °C.

Kinetic measurements. All kinetic experiments were measured in CH_2Cl_2 at -90 °C in a cuvette (containing a magnetic stirbar) with 1 cm pathlength. 11.7 mM of [$Fe^{III}(O)Fe^{III}$poat]$^+$ stock solution, 9.8 mM of [$N(p\text{-}C_6H_4Br)_3$]PF_6 stock solution, and 87 mM of 2,6-di-*tert*-butyl-phenol (DTBP) stock solution were prepared at room temperature. All stock solutions were stored at -35 °C for the duration of the experiment and warmed back to room temperature for 10 min prior to use. A cuvette filled with 2 mL CH_2Cl_2 solvent was sealed with a rubber septum and transferred into the cryostat of the spectrophotometer to equilibrate with the temperature for > 20 min. First, 40 μL of the [$Fe^{III}(O)Fe^{III}$poat]$^+$ stock solution was injected into the cuvette via airtight syringe and mixed for 150-200 sec to give the desired concentration (0.23 mM). Then, the reaction was initiated with injecting 40 μL (0.85 equiv.) of the [$N(p\text{-}C_6H_4Br)_3$]PF_6 stock solution into the cuvette via airtight syringe while closely monitoring the appearance of absorbance features at λ_{max} = 440, 515, 620, 810, ~1100 nm that is indicative of formation of [$Fe^{III}(O)Fe^{IV}$poat]$^{2+}$. Sub-stoichiometric amount of oxidant was added since [$N(p\text{-}C_6H_4Br)_3$]PF_6 also reacts with DTBP. After the spectrum of [$Fe^{III}(O)Fe^{IV}$poat]$^{2+}$ reached equilibrium (t = 150 sec), 75 μL of the DTBP stock solution (10 equiv.) was injected into the cuvette via airtight syringe. The progress of the reaction was monitored by following the decrease in absorbance at 620 nm (Figure S15). After reaction was completed, the mixture in the cuvette ended as clear orange solution.

Under these conditions, the substrate concentration was in excess compared to the complex concentration to provide pseudo first-order reaction conditions. The expression, $\ln[(A_t - A_f)/(A_i - A_f)]$, was plotted against the reaction time for the first three half-lives of any reaction to provide linear

plots. Here, A_i is the initial absorbance, A_t is the absorbance at time t, and A_f is the absorbance at the endpoint of the reaction at 620 nm. The observed pseudo first-order rate constants (k_{obs}, s^{-1}) for the reaction was determined from the slope of the above-mentioned linear plots. We note that controlled experiments were performed for the reactions of DPH and DTBP with $[Fe^{III}(O)Fe^{III}poat]^+$ and $[Fe^{III}(O)Fe^{III}Hpoat]^{2+}$, and no reactivity was observed.

GC-MS experiments. Typically, the solution from a UV-vis kinetics experiment with DPH and DTBP is directly subjected to a GC-MS measurement without further workup (Figures S14, S16). The percent conversion from DTBP to diphenoquinone and bisphenol is calculated by comparing the relative area of diphenoquinone and bisphenol with unreacted DTBP. Additionally, the following factors are taken into account: 1) DTBP was added in 10-fold excess; 2) two equivalents of $[Fe^{III}(O)Fe^{IV}poat]^{2+}$ reacts with two equivalents of DTBP to produce one equivalent of bisphenol, and two equivalents of $[Fe^{III}(O)Fe^{IV}poat]^{2+}$ reacts with one equivalent of bisphenol to produce one equivalent of diphenoquinone; and 3) sub-stoichiometric $[N(C_6H_4Br)_3]PF_6$ (0.8 equiv.) was added to avoid reaction between the unreacted oxidant and DTBP. The percent conversions are calculated to be > 90%.

NMR identification of organic products. $[Fe^{III}(O)Fe^{III}poat]OTf$ (0.0299 g, 0.0251 mmol, 1.0 equiv) was dissolved in 3 mL CH_2Cl_2 and transferred to a 50 mL Schlenk flask in a glove box. The flask was sealed with a septum, brought out of the box, and chilled in a -94 °C bath for 20 minutes. An aliquot of $[N(p\text{-}C_6H_4Br)_3]PF_6$ (0.0150 g, 0.0239 mmol, 0.95 equiv) in 0.25 mL CH_2Cl_2 was added *via* a gas-tight syringe, and the red solution turned dark brownish green immediately and was allowed to stir for 5 minutes. An aliquot of DPH (0.0023 mg, 0.013, 0.52 equiv) in 0.070 mL CH_2Cl_2 was injected *via* a gas-tight syringe, and the brownish green solution turned to dark red. The mixture was allowed to stir for 10 minutes, before warming to room temperature for 1 hour. All volatiles were

removed *in vacuo* using a Schlenk line, and the Schlenk flask was brought back into the glove box. The red residue was triturated with three portions of 20 mL Et_2O, which were combined as a pale yellow solution with minor particulates. The Et_2O solution was filtered to remove the insoluble material, and the solvent was removed *in vacuo* to afford an orange-yellow residue as the organic product. The isolated product was redissolved in 0.65 mL $CDCl_3$ (1% TMS), and the NMR spectrum was collected and illustrated in Figure S13C.

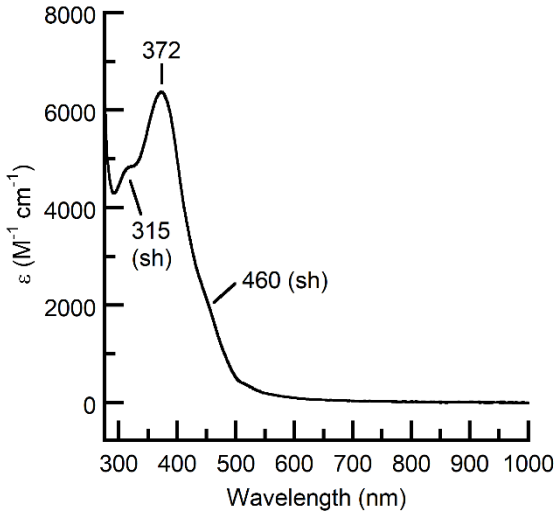

Figure S1. Electronic absorbance spectrum of $[Fe^{II}(OH)Fe^{III}poat]^+$. The spectrum was collected in CH_2Cl_2 at room temperature at a concentration of 0.10 mM.

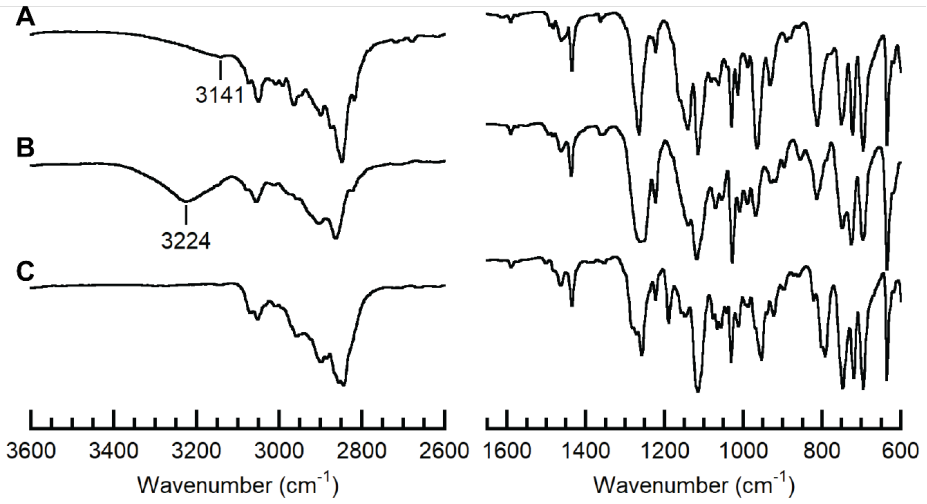

Figure S2. FTIR spectra of $[Fe^{II}(OH)Fe^{III}poat]^{+}$ (A), $[Fe^{III}(O)Fe^{III}Hpoat]^{2+}$ (B), and $[Fe^{III}(O)Fe^{III}poat]^{+}$ (C). The left panel shows the high energy region, and the right panel shows the low energy region.

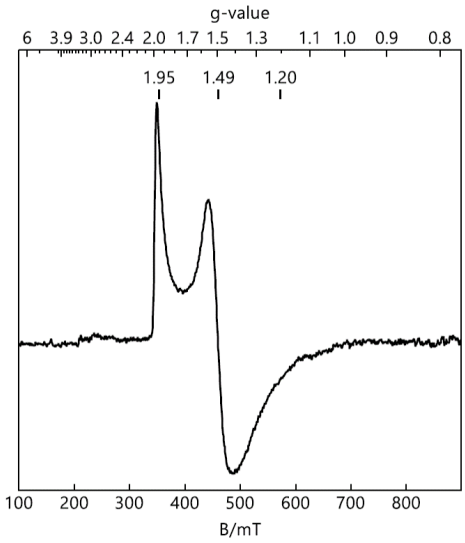

Figure S3. EPR spectrum of $[Fe^{II}(OH)Fe^{III}poat]^{+}$. Microwaves 0.2 mW at 9.634 GHz, temperature 6 K.

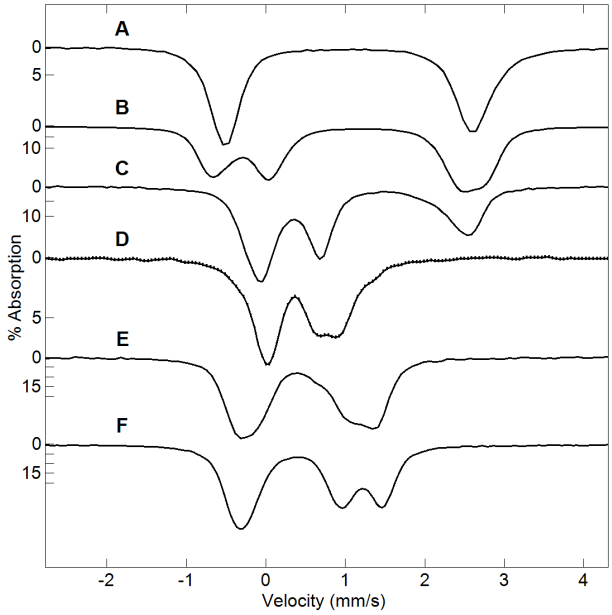

Figure S4. Mossbauer spectra of (A) $[Fe^{II}poat(OH)]^{2-}$, (B) $[Fe^{II}(OH)Fe^{II}poat]$, (C) $[Fe^{II}(OH)Fe^{III}poat]^{+}$, (D) $[Fe^{III}(OH)Fe^{III}poat]^{2+}$, (E) $[Fe^{III}(O)Fe^{III}Hpoat]^{2+}$, (F) $[Fe^{III}(O)Fe^{III}poat]^{+}$. All spectra recorded on frozen solution samples of enriched ^{57}Fe at 4 K (except the spectrum in C which was recorded at 100K) and magnetic field of 45 mT. The spectra are all displayed for equal areas. The $[Fe^{III}(O)Fe^{IV}poat]^{2+}$ species shows a magnetic pattern.

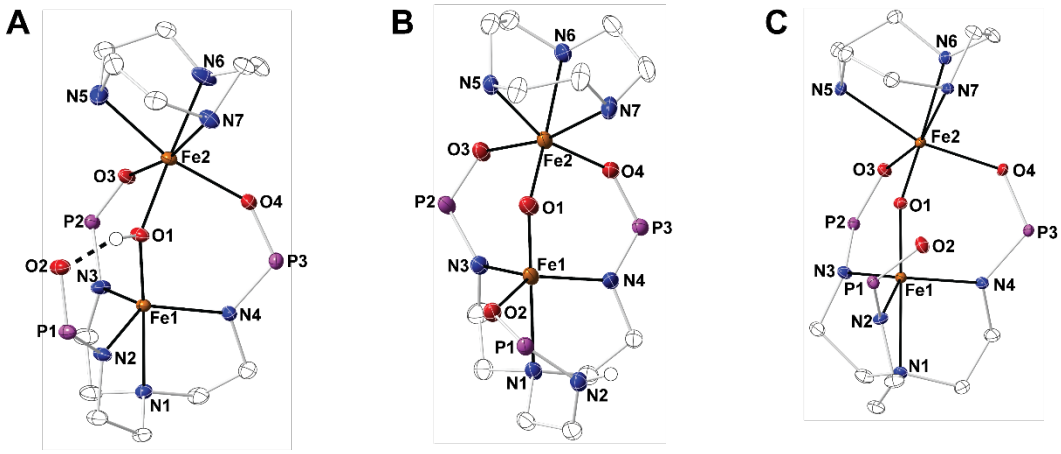

Figure S5. Thermal ellipsoid diagram depicting the molecular structure of $[Fe^{II}(OH)Fe^{III}poat]^{+}$ (A), $[Fe^{III}(O)Fe^{III}Hpoat]^{2+}$ (B) and $[Fe^{III}(O)Fe^{III}poat]^{+}$ (C), where the methyl and phenyl groups are removed, and only the diiron cores are shown for clarity. Ellipsoids are drawn at the 50 % probability level, and only the hydroxido and phosphinic amide H atoms are show for clarity. The triflate counter anions are outer-sphere and are not interacting with the cation.

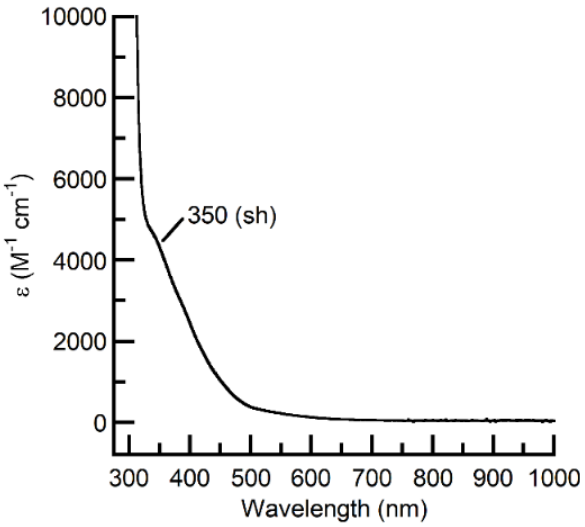

Figure S6. Electronic absorbance spectrum of [Fe^{II}(OH)Fe^{II}poat]. The spectrum was collected in CH_2Cl_2 at room temperature at a concentration of 0.10 mM.

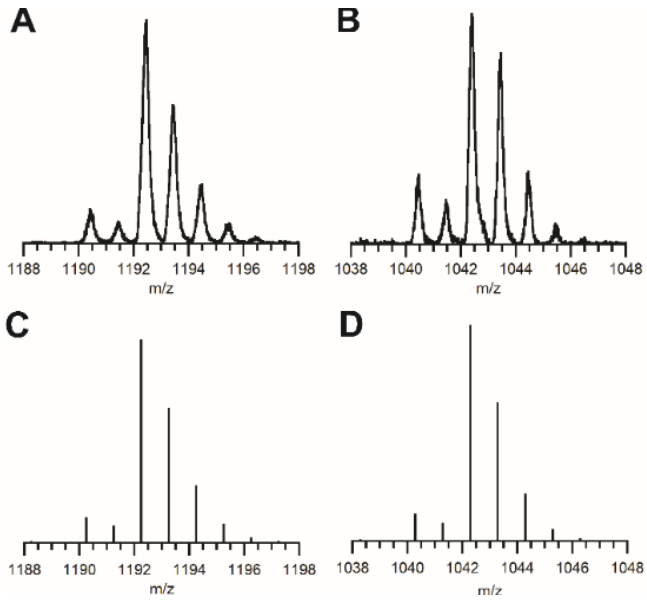

Figure S7. ESI-MS spectra of [Fe^{III}(O)Fe^{III}Hpoat]$^{2+}$ (A) and [Fe^{III}(O)Fe^{III}poat]$^{+}$ (B), with the simulated spectra shown in (C) and (D), respectively.

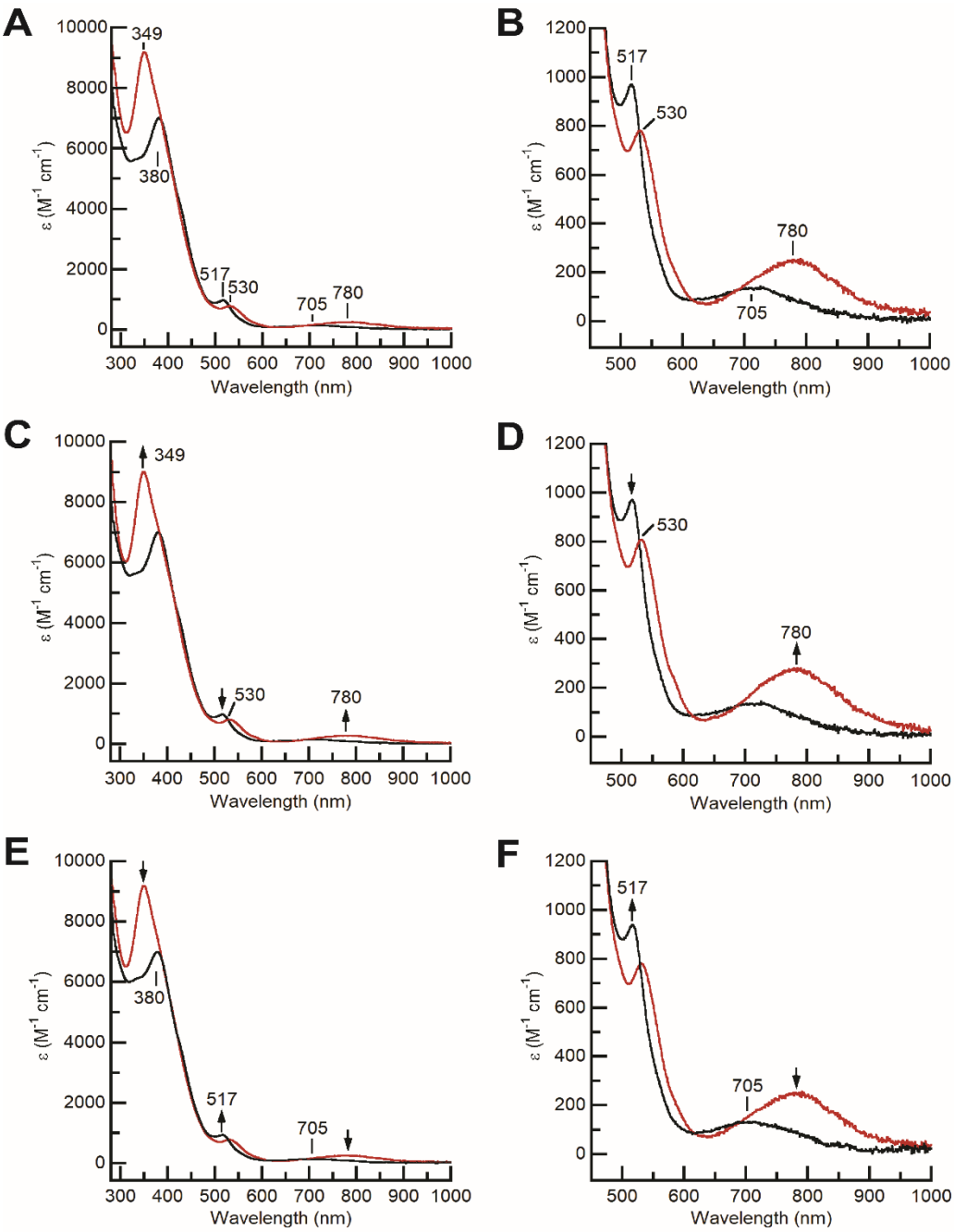

Figure S8. (A) Electronic absorbance spectra of $[Fe^{III}(O)Fe^{III}Hpoat]^{2+}$ (black) and $[Fe^{III}(O)Fe^{III}poat]^{+}$ (red), with (B) showing the low energy features. (C) Electronic absorbance spectra of the deprotonation of $[Fe^{III}(O)Fe^{III}Hpoat]^{2+}$ before (black) and after (red) the addition of NEt_3, with (D) showing the changes in the low energy features. (E) Electronic absorbance spectra of the protonation of $[Fe^{III}(O)Fe^{III}poat]^{+}$ before (red) and after (black) the addition of [2,6-HLut]OTf, with (F) showing the changes in the low energy features. Spectra were collected in CH_2Cl_2 at room temperature at a concentration of 0.10 mM.

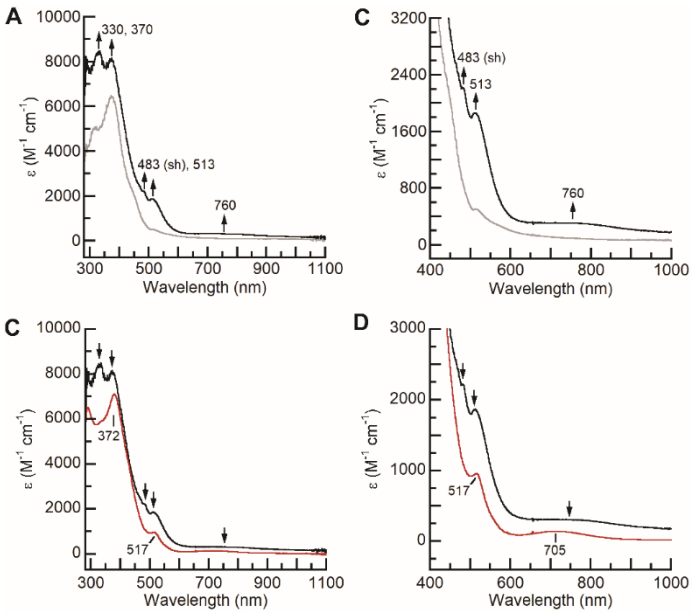

Figure S9. (A) Electronic absorbance spectra of the chemical oxidation of $[Fe^{II}(OH)Fe^{III}poat]^{+}$ before (grey) and after (black) the addition of $[FeCp_2]OTf$ at -80 °C, with (B) showing the changes to the low energy features. (C) Electronic absorbance spectra of the conversion of $[Fe^{III}(OH)Fe^{III}poat]^{2+}$ (black) to $[Fe^{III}(O)Fe^{III}Hpoat]^{2+}$ (red) upon warming from -80 °C to room temperature, with (D) showing the changes to the low energy features. The spectra were collected in CH_2Cl_2 at a concentration of 0.10 mM.

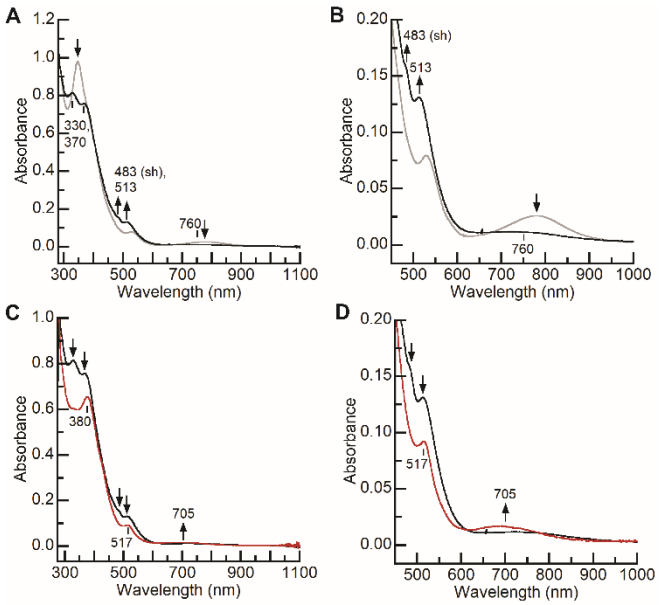

Figure S10. (A) Electronic absorbance spectra of the protonation of $[Fe^{III}(O)Fe^{III}poat]^{+}$ before (grey) and after (black) the addition of [HLut]OTf at -60 °C, with (B) showing the changes to the low energy features. (C) Electronic absorbance spectra of the conversion of $[Fe^{III}(OH)Fe^{III}poat]^{2+}$ (black) to $[Fe^{III}(O)Fe^{III}Hpoat]^{2+}$ (red) upon warming from -60 °C to room temperature, with (D) showing the changes to the low energy features. The spectra were collected in CH_2Cl_2 at a concentration of 0.10 mM.

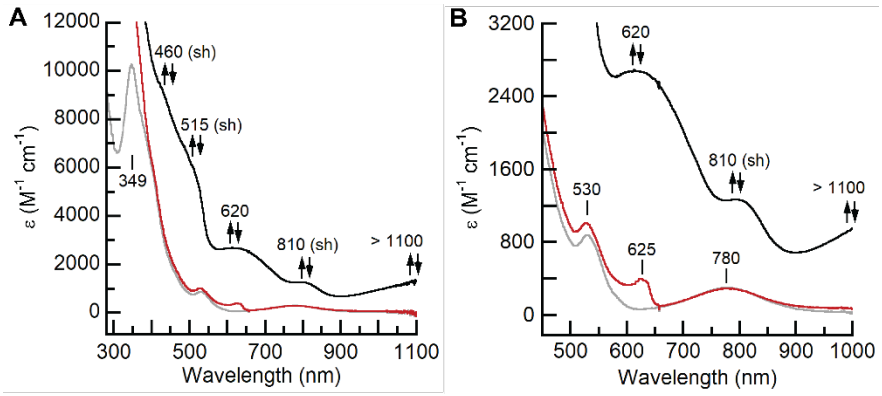

Figure S11. (A) Electronic absorbance spectra of the reversible oxidation of $[Fe^{III}(O)Fe^{III}poat]^{+}$ before (grey) and after (black) the addition of $[N(p\text{-}C_6H_4Br)_3]PF_6$, and after the addition of $FeCp_2$ (red), with (B) showing the changes to the low energy features. The spectra were collected in CH_2Cl_2 at -90 °C at a concentration of 0.10 mM.

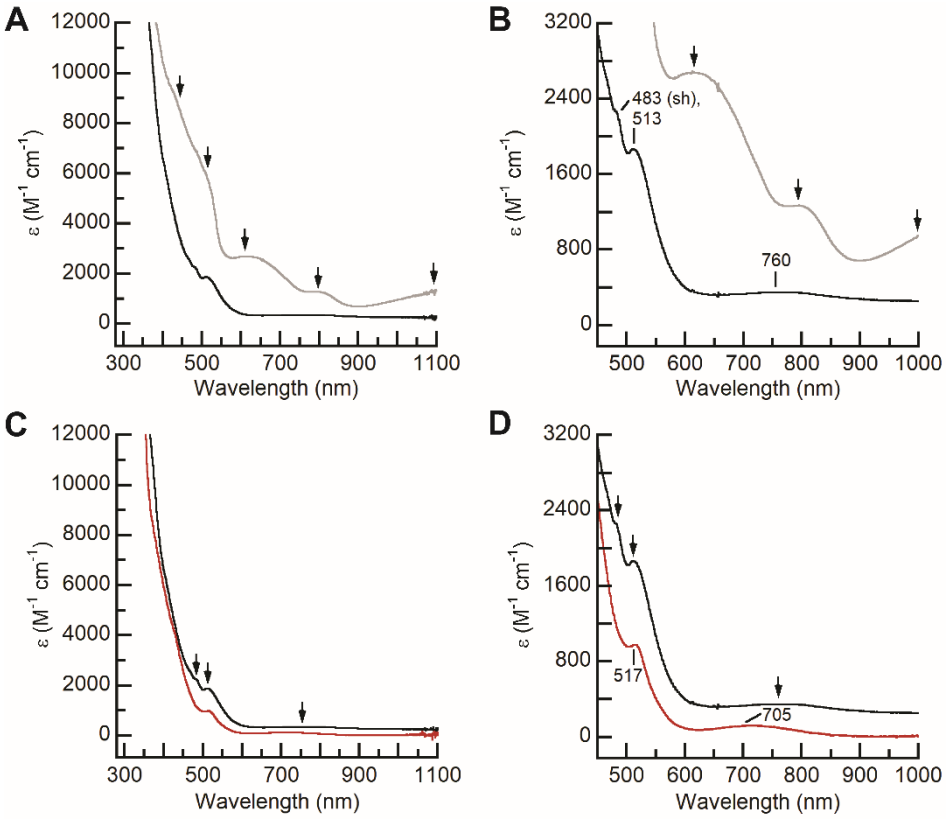

Figure S12. (A) Electronic absorbance spectra of the conversion of $[Fe^{III}(O)Fe^{IV}poat]^{2+}$ before (grey) and after (black) the addition of DPH at -90 °C, with (B) showing the changes to the low energy features. (C) Electronic absorbance spectra of the conversion of $[Fe^{III}(OH)Fe^{III}poat]^{2+}$ (black) to $[Fe^{III}(O)Fe^{III}Hpoat]^{2+}$ (red) upon warming from -90 °C to room temperature, with (D) showing the changes to the low energy features. The spectra were collected in CH_2Cl_2 at a concentration of 0.10 mM.

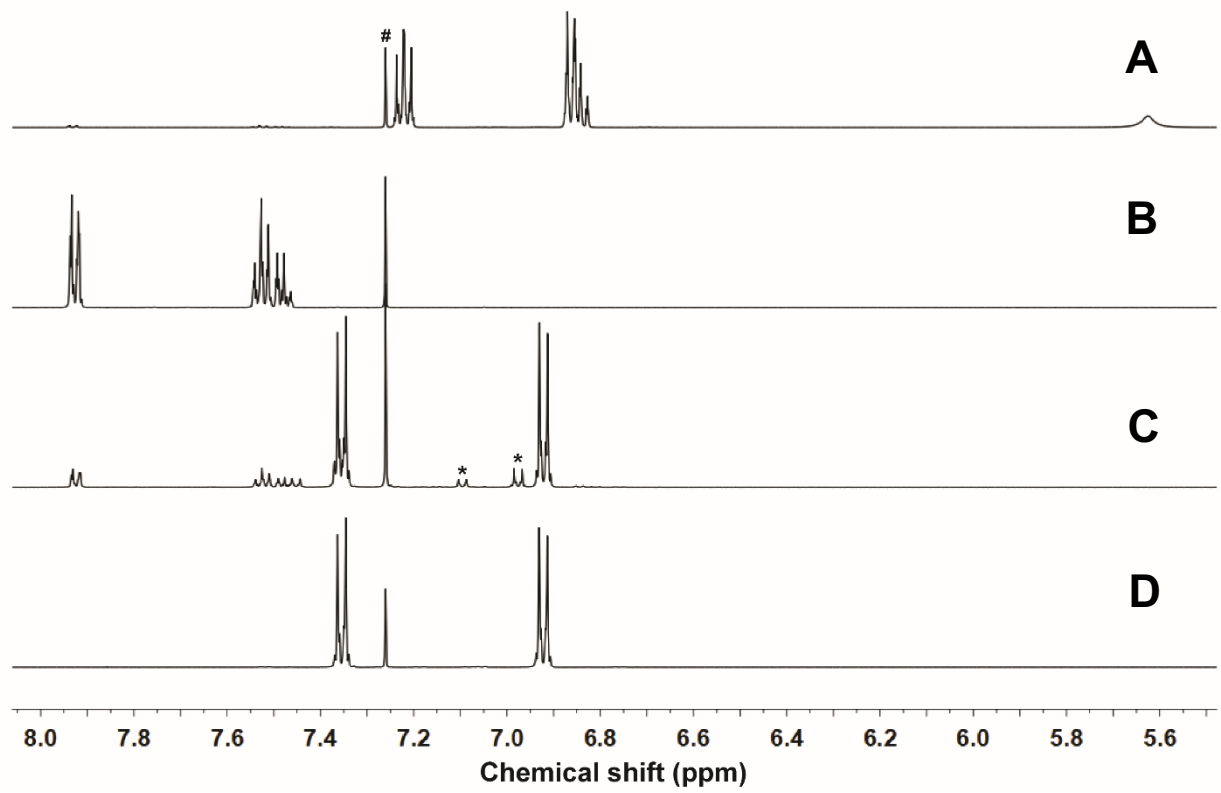

Figure S13. NMR spectra of DPH standard (A), azobenzene standard (B), bulk reaction of $[Fe^{III}(O)Fe^{IV}poat]^{2+}$ and DPH (C), and N(*p*-$C_6H_4Br)_3$ standard (D). Spectra were collected in $CDCl_3$ at room temperature. # indicates $CHCl_3$ solvent peak. * indicates unknown impurities.

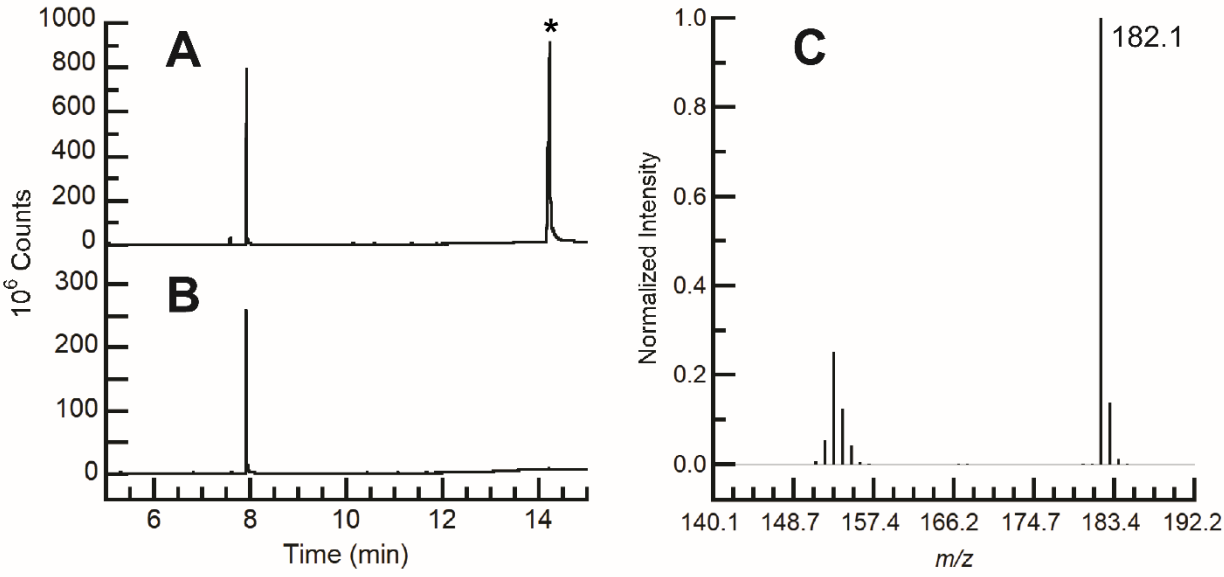

Figure S14. Gas chromatograms of (A) reaction between $[Fe^{III}(O)Fe^{IV}poat]^{2+}$ and DPH, and (B) azobenzene standard. * indicates the oxidant byproduct (N(*p*-$C_6H_4Br)_3$). (C) Mass spectrum of the species detected t = 7.9 min in gas chromatography corresponds to azobenzene (182.1 m/z).

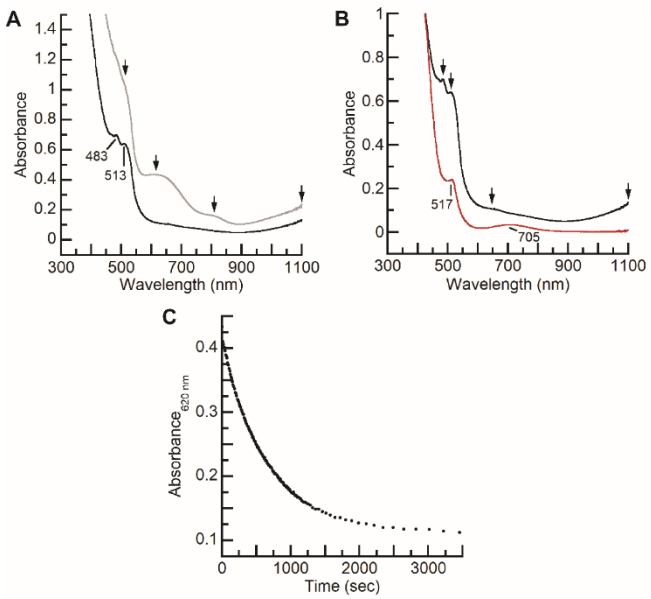

Figure S15. (A) Electronic absorbance spectra of the conversion of $[Fe^{III}(O)Fe^{IV}poat]^{2+}$ before (grey) and after (black) the addition of DTBP at -90 °C. (B) Electronic absorbance spectra of the subsequent conversion of $[Fe^{III}(OH)Fe^{III}poat]^{2+}$ (black) to $[Fe^{III}(O)Fe^{III}Hpoat]^{2+}$ (red) upon warming from -90 °C to room temperature. (C) Time trace of the decrease of the λ_{max} = 620 nm feature upon addition of DTBP. Spectra were collected in CH_2Cl_2 at a concentration of 0.23 mM.

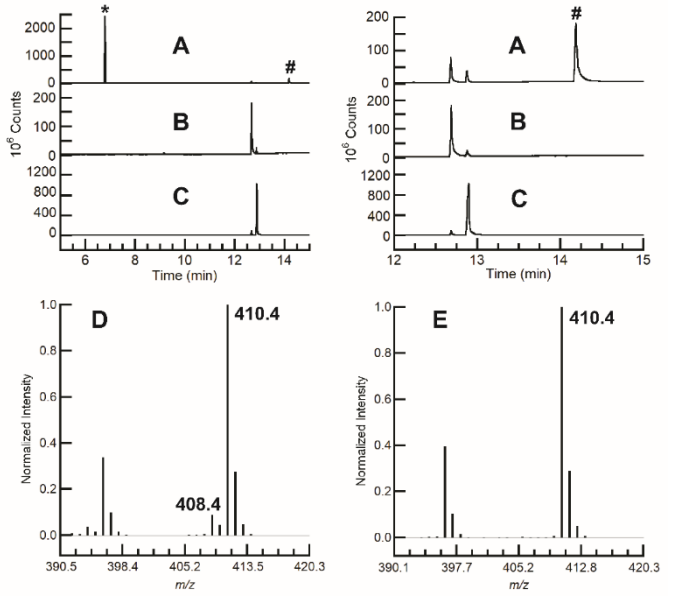

Figure S16. Gas chromatograms of (A) the reaction between $[Fe^{III}(O)Fe^{IV}poat]^{2+}$ and DTBP, (B) diphenoquinone standard, and (C) bisphenol standard. The left panel contains the full chromatograms, and the right panel contains the chromatograms at t = 12 to 15 min. * indicates unreacted DTBP, and # indicates the oxidant byproduct (N(*p*-$C_6H_4Br)_3$). (D) Mass spectrum of the species detected t =12.7 min in gas chromatography corresponds to diphenoquinone (408.4 m/z). (E) Mass spectrum of the species detected t = 12.9 min in gas chromatography corresponds to bisphenol (410.4 m/z).

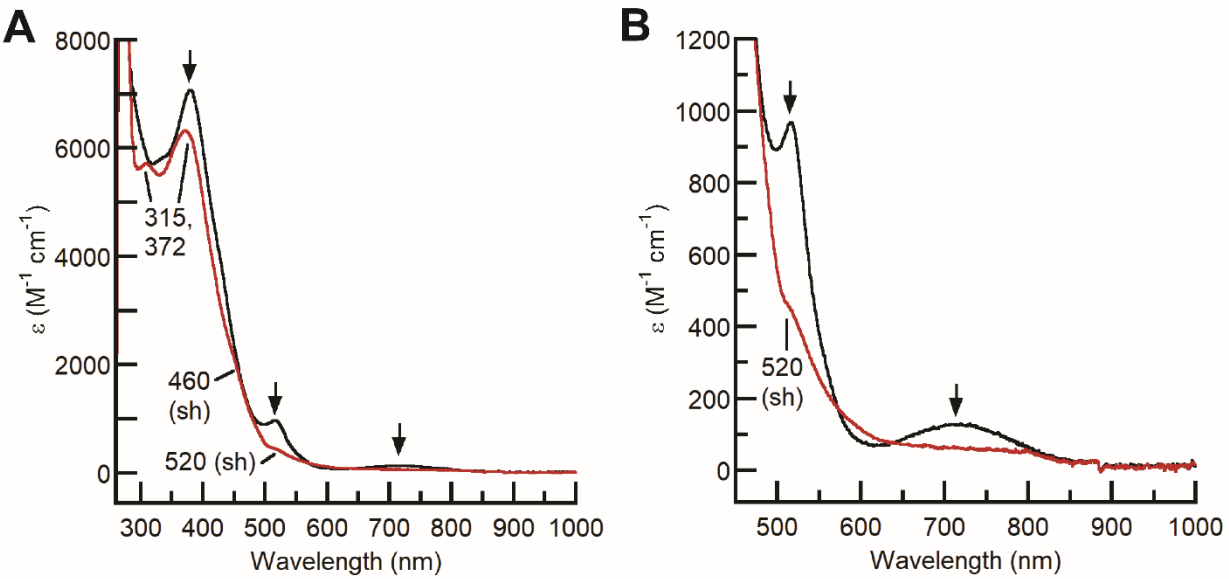

Figure S17. (A) Electronic absorbance spectra of the chemical reduction of $[Fe^{III}(O)Fe^{III}Hpoat]^{2+}$ before (black) and after (red) the addition of $CoCp_2$ at room temperature, with (B) showing the changes to the low energy features. The spectra were collected in CH_2Cl_2 at a concentration of 0.10 mM.

Table S1. Crystallographic data for $[Fe^{II}(OH)Fe^{III}poat]^{+}$, $[Fe^{III}(O)Fe^{III}Hpoat]^{2+}$, and $[Fe^{III}(O)Fe^{III}poat]^{+}$.

	[(TMTACN)Fe^{II}–(μ-OH)–Fe^{III}poat]OTf	[(TMTACN)Fe^{III}–(μ-O)–Fe^{III}Hpoat](OTf)$_2$	[(TMTACN)Fe^{III}–(μ-O)–Fe^{III}poat]OTf
Formula	C_{54} H_{64} F_3 Fe_2 N_7 O_7 P_3 S	C_{54} H_{65} Cl_3 F_6 Fe_2 N_7 O_{10} P_3 S	C_{54} H_{67} Cl_4 F_3 Fe_2 N_7 O_7 P_3 S
fw	1192.77	1461.21	1361.61
T (K)	133(2)	93(2)	93(2)
Crystal system	Triclinic	Monoclinic	Triclinic
Space group	$P\bar{1}$	$P2_1/c$	$P\bar{1}$
a (Å)	14.918(2)	16.6081(6)	10.5370(5)
b (Å)	17.229(3)	14.8447(5)	13.6903(7)
c (Å)	21.457(3)	27.0177(9)	21.8456(11)
α (°)	89.463(3)	90	93.1573(8)
β (°)	89.920(3)	91.9316(6)	101.4197(8)
γ (°)	81.928(3)	90	104.7658(8)
Z	4	4	2
V (Å^3)	5460.0(14)	6657.2(4)	2968.4(3)
δ_{calc} (mg/m^3)	1.451	1.458	1.523
Independent reflections	31868	18665	17414
R1	0.0434	0.0401	0.0539
wR2	0.1027	0.0979	0.1473
Goof	1.020	1.022	1.073
CCDC#	2121051	2121052	2121053

$wR2 = [\Sigma[w(F_o^2-F_c^2)^2] / \Sigma[w(F_o^2)^2]]^{1/2}$
$R1 = \Sigma||F_o|-|F_c|| / \Sigma|F_o|$
Goof = $S = [\Sigma[w(F_o^2-F_c^2)^2] / (n-p)]^{1/2}$ where n is the number of reflections and p is the total number of parameters refined.
The thermal ellipsoid plots are shown at the 50% probability level.

References

(1) Armarego, L. F.; Chai, C. L. L. *Purification of Laboratory Chemicals,* 5th ed.; Elsevier: Oxford, UK, 2003.

(2) Lee, J. L.; Oswald, V. F.; Biswas, S.; Hill, E. A.; Ziller, J. W.; Hendrich, M. P.; Borovik, A. S. Stepwise assembly of heterobimetallic complexes: synthesis, structure, and physical properties. *Dalton Trans.* **2021**, *50*, 8111–8119.

(3) Oswald, V. F.; Lee, J. L.; Biswas, S.; Weitz, A. C.; Mittra, K.; Fan, R.; Li, J.; Zhao, J.; Hu, M. Y.; Alp, E. E.; Bominaar, E. L.; Guo, Y.; Green, M. T.; Hendrich, M. P.; Borovik, A. S. Effects of Non-covalent Interactions on High-spin Fe(IV)-oxido Complexes. *J. Am. Chem. Soc.* **2020**, *142*, 11804–11817.

(4) Blakesley, D. W.; Payne, S. C.; Hagen, K. S. Spin-State Variation in Solid State and Solution of Mononuclear Iron(II) 1,4,7-Trimethyl-1,4,7-triazacyclononane Complexes. *Inorg. Chem.* **2000**, *39*, 1979–1989.

(5) Connelly, N. G.; Geiger, W. E. Chemical Redox Agents for Organometallic Chemistry. *Chem. Rev.* **1996**, *96*, 877–910.
(6) Zhdankin, V. V.; Litvinov, D. N.; Koposov, A. Y.; Luu, T.; Ferguson, M. J.; McDonald, R.; Tykwinski, R. R. Preparation and structure of 2-iodoxybenzoate esters: soluble and stable periodinane oxidizing reagents. *Chem. Commun.* **2004**, 106–107.
(7) Zhdankin, V. V.; Koposov, A. Y.; Litvinov, D. N.; Ferguson, M. J.; McDonald, R.; Luu, T.; Tykwinski, R. R. Esters of 2-Iodoxybenzoic Acid: Hypervalent Iodine Oxidizing Reagents with a Pseudobenziodoxole Structure. *J. Org. Chem.* **2005**, *70*, 6484–6491.
(8) Curley, J. J.; Bergman, R. G.; Tilley, T. D. Preparation and physical properties of early-late heterobimetallic compounds featuring Ir–M bonds (M = Ti, Zr, Hf). *Dalton Trans.* **2012**, *41*, 192–200.
(9) Bell, F. A.; Ledwith, A.; Sherrington, D. C. Cations-radicals: tris-(*p*-bromophenyl)amminium perchlorate and hexachloroantimonate. *J. Chem. Soc. C* **1969**, 2719–2720.
(10) Eberson, L.; Larsson, B. Electron Transfer Reactions in Organic Chemistry. XII. Reactions of 4-Substituted Triarylaminium Radical Cations with Nucleophiles; Polar vs. Electron Transfer Pathways. *Acta. Chemica Scandinavica* **1987**, *B 41*, 367–378.
(11) Weber, B.; Betz, R.; Bauer, W.; Schlamp, S. Crystal Structure of Iron(II) Acetate. *Z. Anorg. Allg. Chem.* **2011**, *637*, 102–107.
(12) Hagadorn, J. R.; Que, L.; Tolman, W. B. N-Donor Effects on Carboxylate Binding in Mononuclear Fe(II) Complexes of a Sterically Hindered Benzoate Ligand. *Inorg. Chem.* **2000**, *39*, 6086–6090.
(13) APEX2 Version 2014.11-0, Bruker AXS, Inc.; Madison, WI 2014.
(14) SAINT Version 8.34a, Bruker AXS, Inc.; Madison, WI 2013.
(15) Sheldrick, G. M. SADABS, Version 2014/5, Bruker AXS, Inc.; Madison, WI 2014.
(16) Sheldrick, G. M. SHELXTL, Version 2014/7, Bruker AXS, Inc.; Madison, WI 2014.
(17) International Tables for Crystallography 1992, Vol. C., Dordrecht: Kluwer Academic Publishers.
(18) (a) Spek, A. L. SQUEEZE, *Acta Cryst.* **2015**, *C71*, 9–19. (b) Spek, A. L. PLATON, *Acta. Cryst.* **2009**, *D65*, 148–155.